https://doi.org/10.5194/egusphere-2026-4748
Preprint. Discussion started: 27 August 2026

Diurnal variations of deep convective cloud physical properties and their relationships with rainfall over South China and adjacent seas

Feng Zhang[1,2], Zhiguo Wang[1], Zhijun Zhao[1,2], Wenwen Li[3], Zhixin Yang[1,2], Haoyang Fu[4]

[1]Key Laboratory of Polar Atmosphere-Ocean-Ice System for Weather and Climate of Ministry of Education/Shanghai Key Laboratory of Ocean-Land-Atmosphere Boundary Dynamics and Climate Change, Department of Atmospheric and Oceanic Sciences & Institutes of Atmospheric Sciences, Fudan University, Shanghai, China.
[2]Key Laboratory for Information Science of Electromagnetic Waves, Ministry of Education, College of Future Information Technology, Fudan University, Shanghai, China.
[3]Engineering Research Center of Optical Instrument and System, the Ministry of Education, Shanghai Key Laboratory of Modern Optical System, University of Shanghai for Science and Technology, Shanghai, China.
[4]College of Physics and Electronic Information Engineering, Zhejiang Normal University, Jinhua 321004, China.
Correspondence to: Feng Zhang (fengzhang@fudan.edu.cn)

Abstract. Deep convective clouds (DCC) play an important role in heavy rainfall and severe weather. However, limited availability of all-day cloud physical property data has hindered understanding of diurnal variations of DCC physical properties and their relationships with rainfall over South China and the adjacent seas. This study investigates diurnal variations of DCC physical properties and their relationships with rainfall using all-day cloud products from the DaYu Cloud Analysis System (DaYu–CLAS). The results show pronounced regional heterogeneity in DCC diurnal variations. Inland and eastern coastal DCC exhibit afternoon peaks, with the eastern coastal region showing larger diurnal amplitudes. Oceanic DCC are active from nighttime to early morning, whereas DCC on the southern flank of the Yungui Plateau exhibit bimodal patterns with early morning and afternoon peaks. Relationships between cloud physical properties and rainfall rate (RR) show similar patterns across subregions. Cloud optical thickness and cloud water path (CWP) are positively correlated with RR, cloud top height shows a nonlinear positive relationship, and cloud effective radius exhibits a threshold-like behavior near 29 μm. Based on these relationships, a machine learning model is established to estimate RR using cloud physical properties, meteorological variables, and geographic location. The model shows reasonable performance across all subregions ($R > 0.64$) and reconstructs general RR diurnal features, with CWP identified as the dominant predictor. These findings improve the understanding of DCC diurnal variations and demonstrate the potential of cloud physical properties for convective rainfall estimation and monitoring.

1 Introduction

Deep convective clouds (DCC) represent the intense precipitating core regions of deep convective systems (Steiner et al., 1995; Feng et al., 2012). The development of DCC is frequently associated with severe convective weather, including heavy rainfall, thunderstorms, and hail. Moreover, DCC play a key role in material exchange between the troposphere and the stratosphere, thereby exerting profound impacts on the global water, energy, aerosol, and chemical cycles (Andreae et al., 2018; Barth et al., 2007; Li et al., 2021; Roca et al., 2010). As the most active component of deep convective systems, DCC play a crucial role in driving vertical transport and regulating the life–cycle evolution of the entire system. In contrast, stratiform precipitation regions are generally broader and less intense, whereas cirrus cloud regions are usually regarded as non-precipitating components of deep convective systems (Houze, 1989, 2004; Lin et al., 2007; Y. Zhao et al., 2024). Given the direct connection between DCC and convective rainfall, this study focuses on the diurnal variation of DCC. Xu（2013), in a study of deep convective rainfall characteristics over East Asia, reported that convective storms over South China exhibit the highest intensity. Under the combined influence of land–sea thermal contrast, complex coastal terrain, and monsoonal flows, the diurnal variation of rainfall in this region exhibits substantial complexity and pronounced regional heterogeneity (Chen et al., 2009). The combined effects of these unique and complex physical processes make South China an ideal region for investigating the diurnal variation of DCC.

In recent years, extensive observations from weather radars, polar-orbiting satellites, and geostationary satellites have made it possible to investigate the spatiotemporal characteristics of DCC at regional and global scales (Masunaga, 2013; Phadtare and Bhat, 2019； Kikuchi and Suzuki, 2019). Using vertical profile information from CloudSat active remote sensing products, Guo and Zhou (2015) found that DCC and cirrus clouds form extensively over southeastern China in summer influenced by the East Asian summer monsoon, replacing the stratocumulus clouds that dominate in winter. However, polar-orbiting satellites have a low sampling frequency over specific regions, making it difficult to fully capture the diurnal variation of DCC. Although weather radars provide high temporal and spatial resolution, their detection coverage is generally limited to land and nearshore areas. For example, Su et al. (2025) combined radar mosaic data with Global Precipitation Measurement (GPM) products and revealed pronounced land–ocean differences in convective scale growth along the coast of South China, with convection over land tending to develop during the daytime and convection over the ocean tending to develop at night. Nevertheless, owing to the limited coverage of radar observations, it remains difficult to examine the evolution of convective systems over broader oceanic regions.

By contrast, geostationary satellites enable continuous observations over broad spatial domains. Zheng and Chen (2013) used long-term geostationary satellite brightness temperature (BT) data to investigate the spatial distribution and multiscale temporal variability of summer deep convection over South China and the adjacent seas. Their results showed that deep convection identified using BT < −52 °C propagates from the ocean to land in the afternoon and from land to ocean around midnight, indicating a distinct diurnal cycle. Similar BT–based approaches have also been widely applied to the identification and tracking of mesoscale convective systems at regional and global scales (Feng et al., 2021; Fiolleau and Roca, 2013). However, BT is not directly related to cloud thickness or rainfall intensity, and it is difficult to effectively separate convective cores from anvil clouds using BT alone (Rickenbach and Rutledge, 1998). To address this issue, Li et al. (2021) proposed a convective tracking approach using dual thresholds of cloud optical thickness (COT) and cloud top height (CTH). Their study demonstrated that incorporating COT and CTH thresholds improves convective identification and tracking compared with the use of a BT threshold alone. However, operational retrievals of cloud physical property products, such as cloud effective radius

https://doi.org/10.5194/egusphere-2026-4748
Preprint. Discussion started: 27 August 2026

(CER) and COT, from the Himawari-8/Advanced Himawari Imager mainly rely on visible and near-infrared channels (Kawamoto et al., 2001; Nakajima and Nakajma, 1995), and are therefore generally available only during daytime. The DaYu Cloud Analysis System (DaYu-CLAS) was developed to address the limitation of nighttime cloud physical property products. This system integrates several advanced deep learning models, including Cloud-ResUNet, CloudDiff, and Cloud-SmaAtUNet for single-layer cloud retrieval, providing continuous all-day cloud physical property products (Li et al., 2023; Tong et al., 2023; Xiao et al., 2025; Z. Zhao et al., 2023, 2024; L. Zhao et al., 2026). DaYu-CLAS provides all-day, high spatiotemporal resolution cloud products, enabling the investigation of DCC diurnal variations of cloud physical properties and the relationships between cloud physical properties and rainfall.

This study uses all-day cloud products from DaYu-CLAS and applies the Tracking of Organized Convection Algorithm through a three-dimensional segmentatioN by incorporating Cloud Physical Properties (TOOCAN-CPP; Li et al., 2021; Z. Zhao et al., 2025) method to systematically investigate the diurnal variations of DCC physical properties and their relationships with rainfall over South China and the adjacent seas. Specifically, this study focuses on two aspects. First, considering differences in topography, underlying surface conditions, and regional meteorological environments, the study region is divided into four subregions to investigate the spatial heterogeneity of DCC diurnal variations and cloud–rainfall relationships. Second, a rainfall rate (RR) estimation model is established based on cloud physical properties, meteorological variables, and geographic information to evaluate the application potential of cloud physical properties for rainfall estimation and their capability to reconstruct regional diurnal rainfall variations.

2 Data and methods

The analysis was conducted during the summer months of 2016–2019 (June–August), with the study region covering South China and the adjacent seas (18°–30° N, 106°–122° E). Figure 1a shows the complex terrain of the study region. It is connected to the Yungui Plateau in the west, contains several major mountain ranges in the inland area and is bordered to the south by the Beibu Gulf and the South China Sea. The complex terrain and land–sea distribution are important factors influencing the initiation, development, and evolution of DCC in this region. To analyze differences in the diurnal variations of DCC under different topography, underlying surface conditions, and regional meteorological backgrounds, the study region is further divided into four subregions (Fig. 1b).

https://doi.org/10.5194/egusphere-2026-4748
Preprint. Discussion started: 27 August 2026

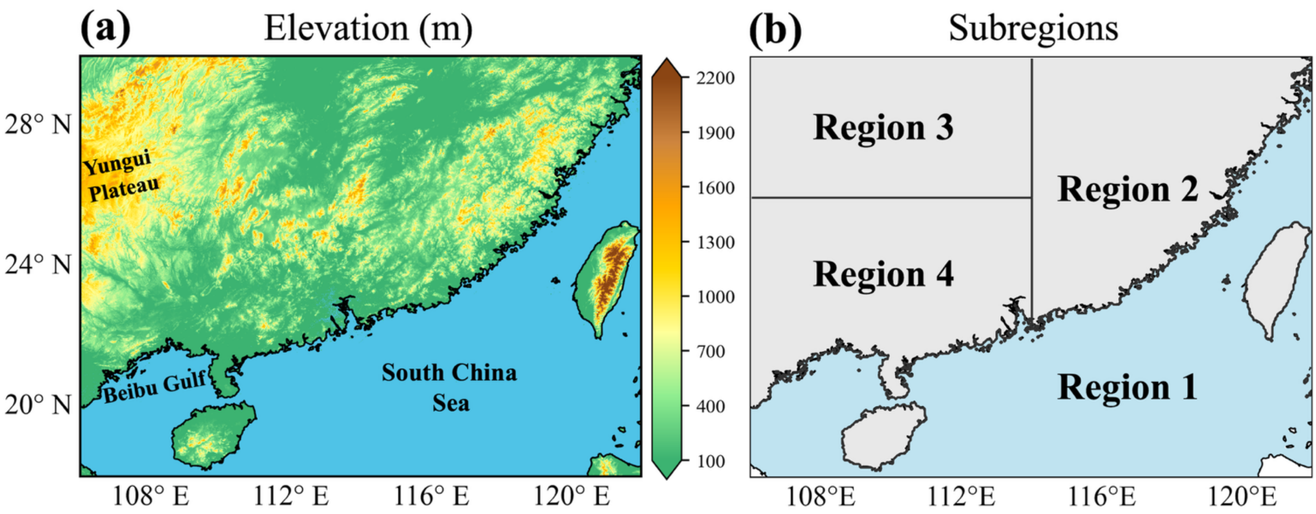

Figure 1. Topography of the study region (a). The study region is divided into four subregions (b): Region 1 denotes the ocean, Region 2 denotes the eastern coastal area, Region 3 denotes the inland area, and Region 4 denotes the southern flank of the Yungui Plateau.

2.1 Data source

The cloud physical properties used in this study were obtained from the DaYu-CLAS cloud products and used to identify and track DCC, characterize their diurnal variations, and analyze cloud–rainfall relationships. These products have a spatial resolution of 0.05° × 0.05° and a temporal resolution of 30 min, including COT, CTH, CER, and cloud phase (CLP). Rainfall data were provided by the Integrated Multi-satellite Retrievals for GPM (IMERG) products to derive DCC rainfall rate and rainfall amount. Meteorological fields were obtained from European Centre for Medium-Range Weather Forecasts Reanalysis v5 (ERA5) to investigate environmental conditions associated with DCC diurnal variations. The ERA5 variables include 2 m temperature (T2m), convective available potential energy (CAPE), 925 hPa wind and divergence, 850 hPa vertical velocity, and total column water vapor (TCWV). Table 1 provides an overview of the datasets used in this study. All datasets span the summer period (June–August) from 2016 to 2019.

https://doi.org/10.5194/egusphere-2026-4748
Preprint. Discussion started: 27 August 2026

Table 1. Description of datasets used in this study.

Variable	Source	Spatial resolution	Temporal resolution
Cloud top height Cloud optical thickness Cloud effective radius Cloud phase	DaYu-CLAS	0.05° × 0.05°	30 min
Temperature (2m) Convective available potential energy Vertical velocity (850 hPa) Divergence and wind (925 hPa) Total column water vapor	ERA5	0.25° × 0.25°	1 hour
Rainfall rate	GPM IMERG	0.1° × 0.1°	30 min

2.2 Research framework and methods

DCC were identified and tracked over the study region using the TOOCAN-CPP method, and the workflow is illustrated in Fig. 2a. First, cloud pixels with CTH > 7 km and COT > 23 were identified as DCC (Li et al., 2021; Liu et al., 2025; Z. Zhao et al., 2025) and then tracked using region-growing method, which considers both spatial connectivity and temporal continuity. Previous studies have applied the TOOCAN-CPP method for DCC identification and tracking across East Asia and the Tibetan Plateau (Li et al., 2021; Z. Zhao et al., 2025). DCC with lifetimes longer than 96 h or maximum equivalent radii exceeding 500 km were excluded to minimize the influence of typhoons and other large-scale weather systems. Finally, 317,591 DCC were obtained, including 94,106, 79,805, 52,362, and 91,318 DCC in Regions 1–4, respectively.

Harmonic analysis method was then applied to characterize the spatiotemporal variations of DCC characteristics, including frequency, rainfall amount, and rainfall rate. Meteorological fields were analyzed to investigate the associated environmental mechanisms. Considering differences in topography, underlying surface conditions, and meteorological backgrounds, the study region was further divided into four subregions to investigate regional differences in DCC diurnal variations (Fig. 2b). Finally, the relationships between cloud physical properties (COT, CTH, CER, and cloud water path, CWP) and RR were analyzed. An XGBoost-based machine learning model was established to estimate RR. Feature importance was evaluated to identify the dominant predictors, and the model was further assessed for its ability to reconstruct the diurnal variations of RR (Fig. 2c). In this study, CWP was estimated from COT and CER using empirical formulas. Different formulations were applied for liquid and ice clouds. The empirical formulas follow previous studies (Liou, 2002; Liu et al., 2025; Nakajima and Nakajma, 1995).

https://doi.org/10.5194/egusphere-2026-4748
Preprint. Discussion started: 27 August 2026

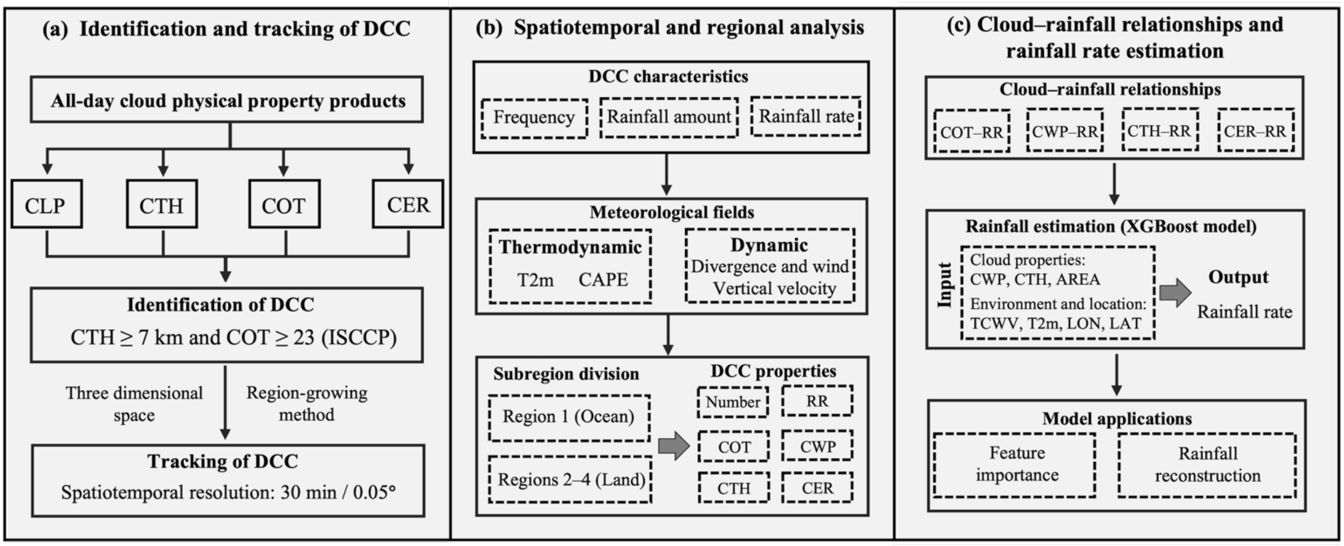

Figure 2. Research framework and workflow.

3 Results and discussion

3.1 Spatiotemporal variations of DCC characteristics and meteorological fields

Figure 3 shows the diurnal amplitude and mean state of DCC characteristics derived from harmonic analysis method, indicating the strength of diurnal variation and the daily mean state, respectively (Dai and Deser, 1999; Roy and Balling, 2005; Love et al., 2011). The harmonic analysis procedure is described in detail in Appendix B. The diurnal amplitude of DCC frequency exhibits pronounced spatial heterogeneity, with large amplitudes mainly distributed along coastal land regions, Taiwan Island, and Hainan Island, while relatively weak amplitudes occur over the open ocean (Fig. 3a). The spatial distribution of the diurnal amplitude of rainfall amount is highly consistent with that of DCC frequency (Fig. 3b). In contrast, large amplitudes of rainfall rate occur not only along eastern coastal land but also widely over oceanic regions (Fig. 3c). In terms of the mean state, DCC frequency over land is generally higher than that over the ocean (Fig. 3d), whereas the mean rainfall amount does not exhibit a clear land-dominant pattern (Fig. 3e). Combined with the distribution of mean rainfall rate, this indicates that oceanic DCC have higher rainfall rate than land (Fig. 3f). Therefore, although DCC occur more frequently over land, stronger rainfall rate over oceanic DCC partly compensates for the land-ocean asymmetry in DCC frequency and reduces the contrast in DCC rainfall amount between land and ocean.

https://doi.org/10.5194/egusphere-2026-4748
Preprint. Discussion started: 27 August 2026

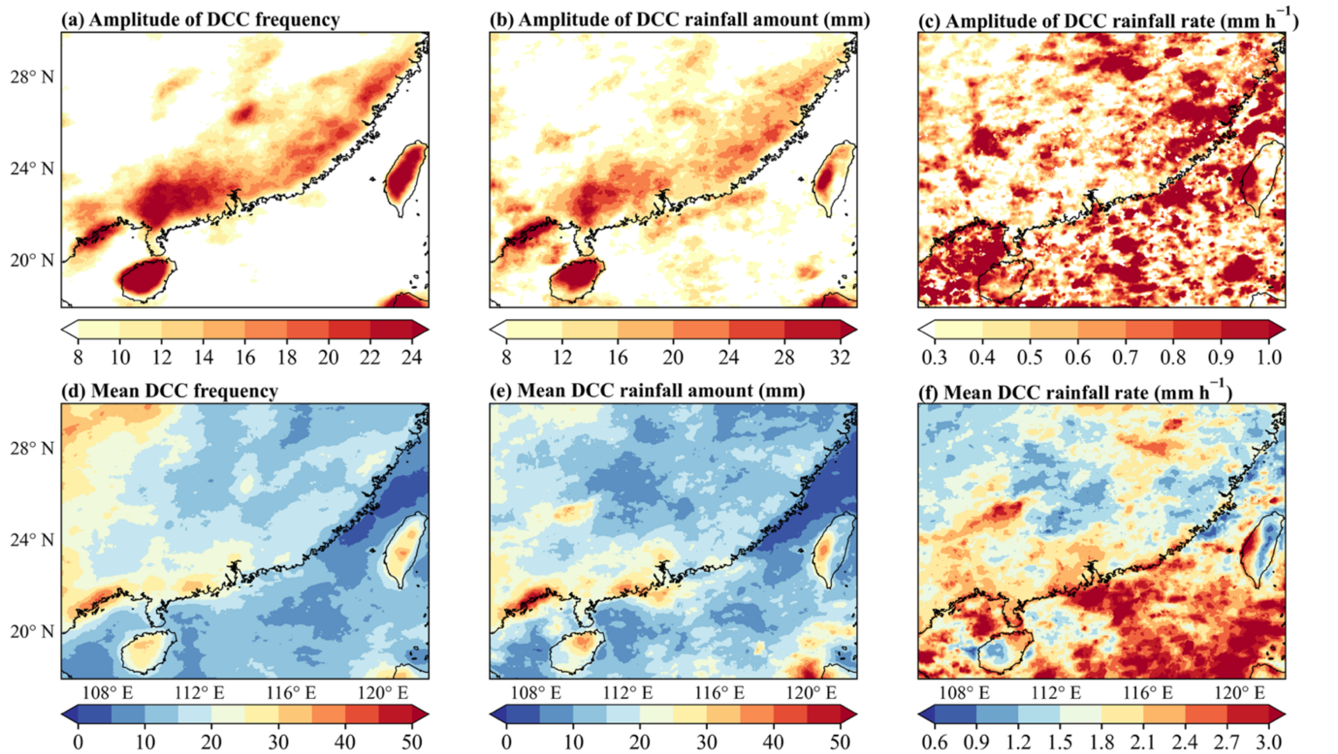

Figure 3. Spatial distributions of the diurnal amplitude and mean state of DCC characteristics derived from harmonic analysis, including DCC frequency (a, d), DCC rainfall amount (b, e), and DCC rainfall rate (c, f).

The spatial distributions of DCC frequency, rainfall amount, and rainfall rate at different time periods are shown in Fig. 4, and the corresponding variations of ERA5 meteorological fields are presented in Fig. 5. During the afternoon period (05:00-09:00 UTC), solar heating over land enhances atmospheric instability, with CAPE reaching relatively high values over land regions (Fig. 5e, f). Meanwhile, a pronounced 925 hPa sea breeze convergence zone and 850 hPa upward motion band develop along the coastal land areas (Fig. 5g, h). Under the combined effects of thermodynamic instability and dynamic convergence, DCC frequency, rainfall amount, and rainfall rate over land observe large values, mainly distributed along coastal land areas, Hainan Island and Taiwan Island (Fig. 4d-f). Previous studies have suggested that afternoon convective rainfall in coastal regions is influenced not only by solar heating but also by sea breeze circulation. (Simpson et al., 2007; Chen et al., 2016). During the evening period (10:00-14:00 UTC), as solar heating weakens, the land surface cool rapidly, CAPE decreases, and the coastal convergence and upward motion bands gradually dissipate (Fig. 5i-l). This environmental transition becomes unfavorable for the development of land DCC, leading to a rapid decrease in DCC frequency, rainfall amount, and rainfall rate, particularly over coastal land areas (Fig. 4g-i).

https://doi.org/10.5194/egusphere-2026-4748
Preprint. Discussion started: 27 August 2026

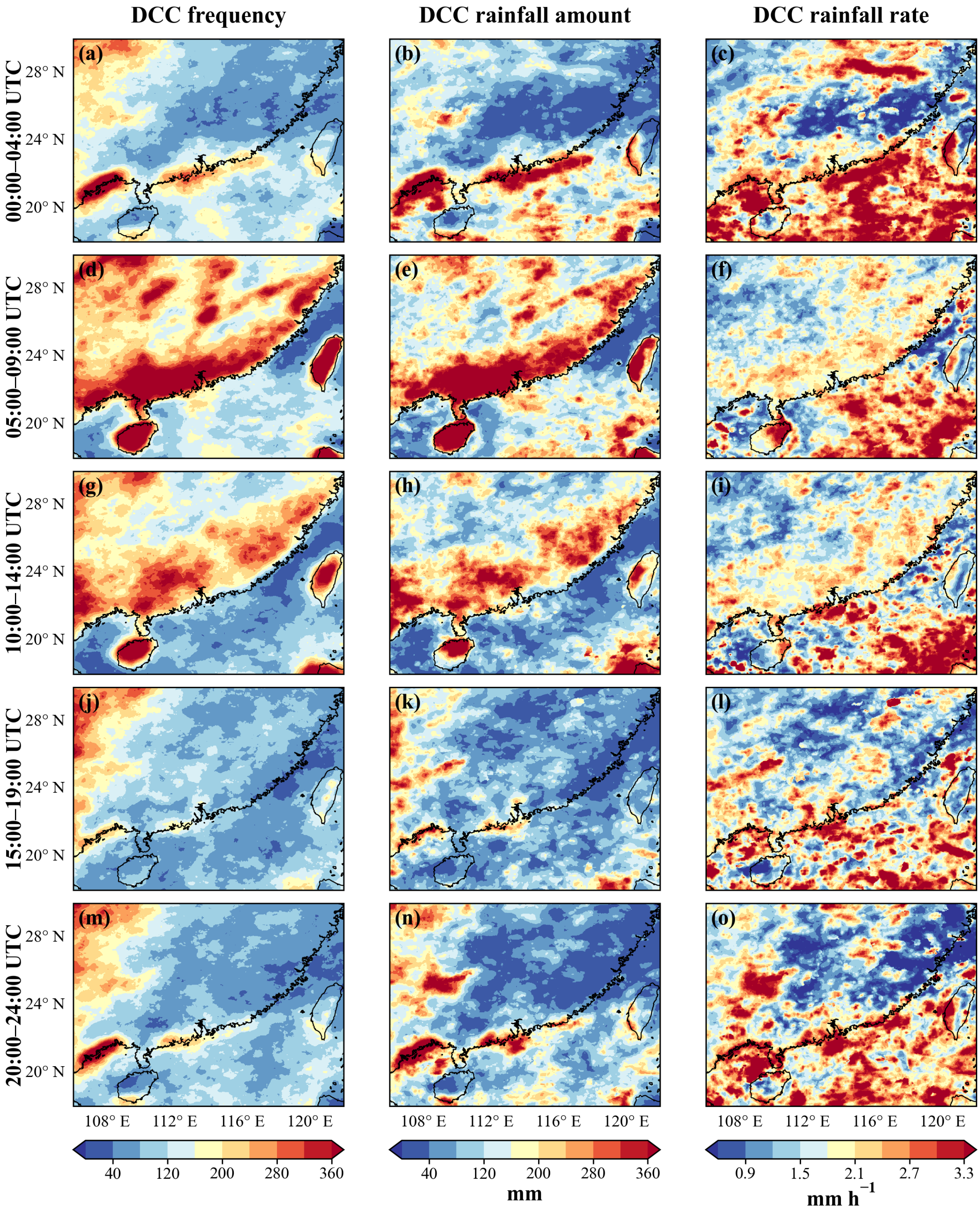

160 **Figure 4. Spatiotemporal variations in DCC characteristics during different time periods, including DCC frequency (a, d, g, j, m), DCC rainfall amount (b, e, h, k, n), and DCC rainfall rate (c, f, i, l, o).**

https://doi.org/10.5194/egusphere-2026-4748
Preprint. Discussion started: 27 August 2026

From late night to early morning (15:00-24:00 UTC), DCC activity exhibits pronounced regional differences. Although thermodynamic conditions over land generally weaken (Fig. 5m, n), DCC activity increases over the southern flank of the Yungui Plateau and along the Beibu Gulf coast (Fig. 4m-o). This enhancement is likely associated with local dynamic processes. The 925 hPa low-level jet (LLJ) near the Beibu Gulf intensifies at night and extends northward toward the southern flank of the Yungui Plateau. Previous studies have shown that nocturnal LLJ intensification is related to inertial oscillations induced by the diurnal variation of turbulence over the upstream Indochina Peninsula (Kong et al., 2020). When the intensified nocturnal jet interacts with the terrain on the southern flank of the Yungui Plateau, a 925 hPa convergence zone develops (Fig. 5o, s), accompanied by enhanced 850 hPa upward motion (Fig. 5p, t). These dynamic processes may partly offset the unfavorable effects of weakened thermodynamic conditions and contribute to nocturnal DCC maintenance and development. Meanwhile, due to the large heat capacity of the ocean, the diurnal amplitudes of DCC frequency and rainfall amount over oceanic regions are relatively weak, consistent with the patterns shown in Fig. 3a and b. However, oceanic CAPE remains relatively high at night (Fig. 5j, n, r). This may partly explain the enhancement of oceanic DCC rainfall rate from nighttime to morning (Fig. 4c, l, o). During the morning period (00:00–04:00 UTC), the Beibu Gulf LLJ gradually weakens, and the low-level convergence and upward motion bands over the southern flank of the Yungui Plateau weaken. At the same time, land areas begin to warm, and CAPE recovers, marking the beginning of a new diurnal cycle.

In summary, the diurnal variations of DCC characteristics exhibit not only pronounced land-ocean contrasts but also strong modulation by local processes, including sea breeze convergence, nocturnal low-level jets, and terrain. The pronounced spatial heterogeneity among different land regions further highlights the need for regional analysis to clarify differences in the diurnal variations of DCC properties and their underlying physical mechanisms under different environmental backgrounds.

https://doi.org/10.5194/egusphere-2026-4748
Preprint. Discussion started: 27 August 2026

180

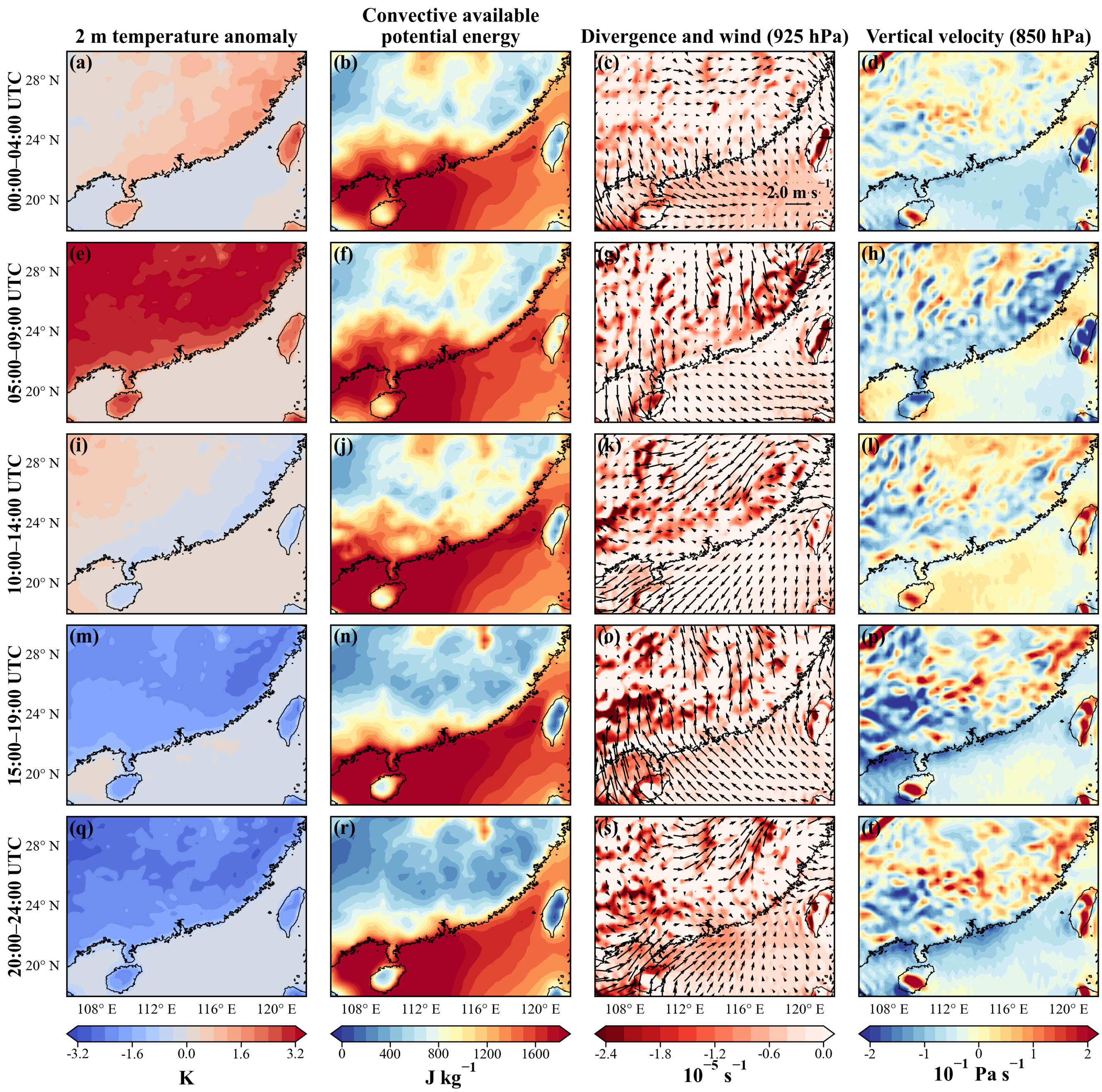

Figure 5. Spatiotemporal variations in ERA5 meteorological fields during different time periods, including 2 m temperature anomaly (a, e, i, m, q), convective available potential energy (b, f, j, n, r), 925 hPa divergence and wind anomaly (c, g, k, o, s), and 850 hPa vertical velocity (d, h, l, p, t).

https://doi.org/10.5194/egusphere-2026-4748
Preprint. Discussion started: 27 August 2026

3.2 Diurnal variations of DCC properties over different subregions

The analysis in Sect. 3.1 identified pronounced spatial heterogeneity in the diurnal variations of DCC characteristics. To further investigate differences in the diurnal variations of DCC properties, including DCC number, RR, COT, CWP, CTH, and CER, under different environmental backgrounds, the study region is divided into four subregions based on topography, underlying surface conditions, and regional meteorological backgrounds (Fig. 1b). A regional comparative analysis is then conducted.

DCC over the ocean (Region 1) exhibit a pronounced active phase from nighttime to early morning. DCC number begins to increase at night and reaches its peak at approximately 07:00 local solar time (LST), followed by a minimum during the afternoon to evening period (16:00–19:00 LST; Fig. 6a). RR shows a similar nocturnal enhancement, but its peak occurs slightly later, at approximately 09:00–10:00 LST (Fig. 6e). In terms of cloud physical properties, both COT and CWP increase continuously from late night to early morning. Specifically, COT reaches its peak at approximately 07:00 LST, showing a phase difference relative to the RR peak. In contrast, CWP peaks during 08:00–10:00 LST and is more synchronized with RR (Fig. 6i, m). The nocturnal enhancement of oceanic DCC may be associated with cloud top longwave radiative cooling (Lee et al., 2020; Liu et al., 2025). In addition, CTH and CER over the ocean both reach their maxima in the afternoon (Fig. 6q, u).

In contrast to the oceanic region, DCC number and RR over the inland region (Region 3) exhibit a typical single afternoon peak. Both variables remain low or decrease from nighttime to early morning, begin to increase rapidly at approximately 10:00 LST, and reach their maxima in the afternoon (Fig. 6c, g). Correspondingly, COT, CWP, CTH, and CER also show highly consistent single-peak diurnal patterns, with peaks mainly concentrated during 15:00–18:00 LST (Fig. 6k, o, s, w). This result is consistent with Li et al. (2021) regarding the semidiurnal variation of deep convective systems, indicating that solar heating is an important factor contributing to the afternoon development of land DCC.

DCC properties over the eastern coastal area (Region 2) also show a single afternoon peak. However, their diurnal amplitudes are larger than those over the inland region, in agreement with the results shown in Fig. 3. These larger diurnal amplitudes may be related to the combined effects of thermodynamic and dynamic processes. In the afternoon, solar heating enhances thermodynamic instability, while sea breeze circulation promotes low-level convergence and upward motion along the coastal areas (Fig. 5e–h), which together may contribute to stronger afternoon DCC development and larger diurnal amplitudes.

Over the southern flank of the Yungui Plateau (Region 4), DCC RR, COT, and CWP exhibit distinctive bimodal patterns (Fig. 6h, l, p). The afternoon peak occurs at approximately 16:00 LST and is mainly associated with solar heating, similar to the mechanism over the inland region. By contrast, the early morning peak, occurring at approximately 07:00 LST, is likely modulated by dynamic processes. At night, the intensified Beibu Gulf LLJ interacts with the terrain on the southern flank of the Yungui Plateau, which is associated with enhanced low-level convergence and upward motion (Fig. 5o, p). This dynamic lifting likely contributes to the maintenance and development of DCC from nighttime to early morning.

https://doi.org/10.5194/egusphere-2026-4748
Preprint. Discussion started: 27 August 2026

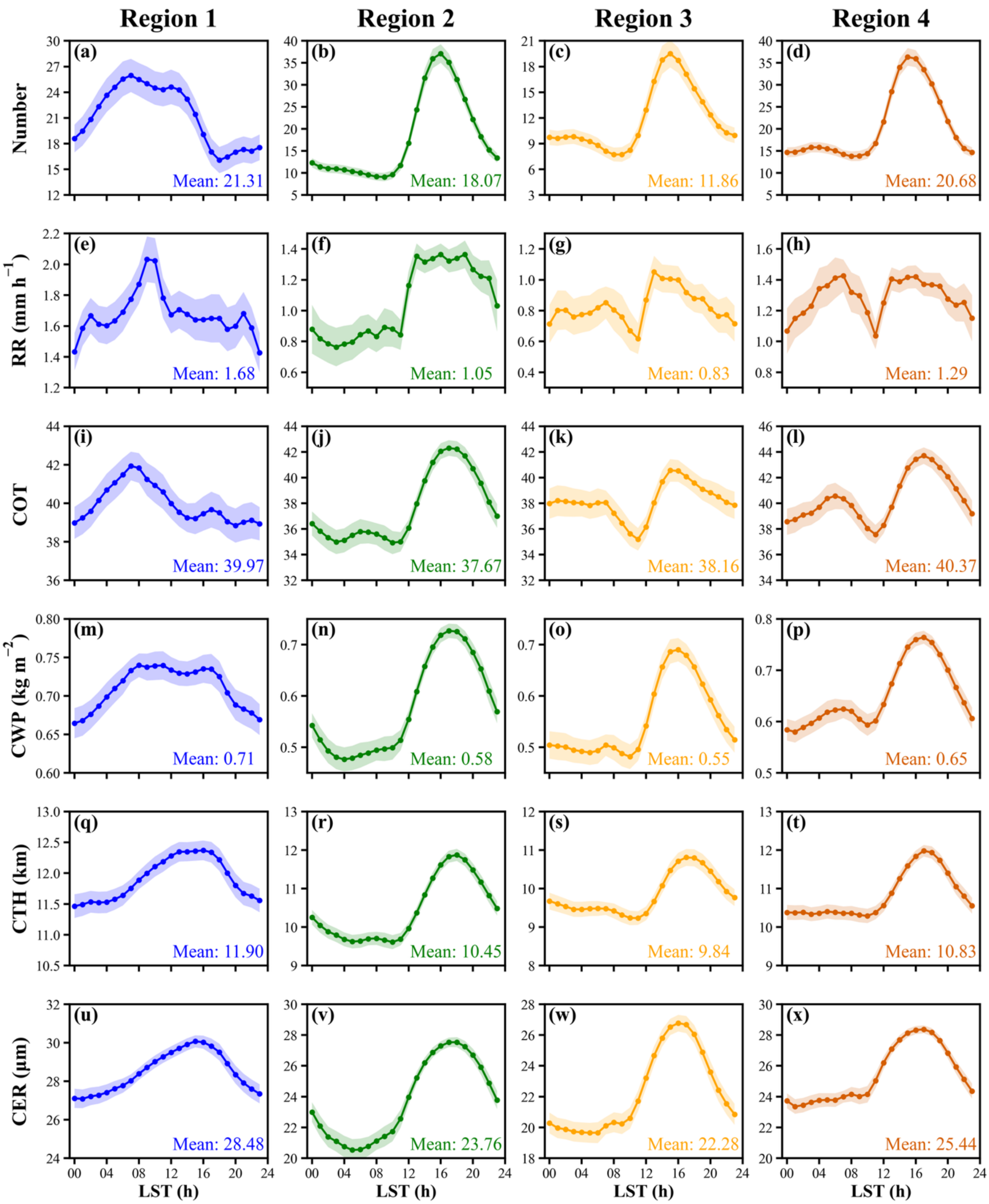

Figure 6. Diurnal variations in DCC properties over the four subregions, including DCC number (a–d), RR (e–h), COT (i–l), CWP (m–p), CTH (q–t), and CER (u–x). The values in the bottom-right corner of each panel represent the mean value of each variable.

https://doi.org/10.5194/egusphere-2026-4748
Preprint. Discussion started: 27 August 2026

3.3 Cloud-rainfall relationships and rainfall estimation

Figure 7 shows the scatter-density plot between DCC cloud physical properties, including COT, CWP, CTH, and CER, and RR across the whole study region. The corresponding results for each subregion are shown in Fig. A1.

As shown in Fig. 7a and b, COT and CWP are strongly positively correlated with RR, with Pearson correlation coefficients (R) of 0.60 and 0.62, respectively. Notably, higher COT and CWP values are accompanied by larger ice cloud fraction, while mean RR continues to increase with COT and CWP, indicating that the increasing fraction of ice-phase clouds does not weaken the positive relationships between COT, CWP, and RR. CTH is also positively correlated with RR (R = 0.47), but the relationship exhibits clear nonlinearity: the increase in RR becomes more rapid as CTH increases (Fig. 7c). This result is in line with the finding of Kubar and Hartmann (2008), who reported that tropical oceanic convective rainfall rate increases rapidly with CTH, particularly for clouds higher than 12 km.

In contrast, the relationship between CER and RR exhibits a complex nonlinear threshold behavior (R = 0.33; Fig. 7d). RR increases with CER when CER is relatively small, reaches a maximum around 29 μm, and then gradually decreases with further increases in CER. This indicates that the relationship between cloud particle size and rainfall intensity is not monotonic, with larger CER values not necessarily corresponding to stronger RR. Similar threshold effects have also been reported in studies of convective storms and precipitating clouds, where heavy precipitation events are often concentrated within a specific CER range, possibly due to the transition from mixed-phase to ice-phase clouds (Cattani et al., 2009; Zheng et al., 2021).

Figure A1 shows that the relationships between cloud physical properties and RR exhibit similar patterns across the four subregions (Regions 1–4), suggesting that these cloud–rainfall relationships are generally consistent within the study region.

https://doi.org/10.5194/egusphere-2026-4748
Preprint. Discussion started: 27 August 2026

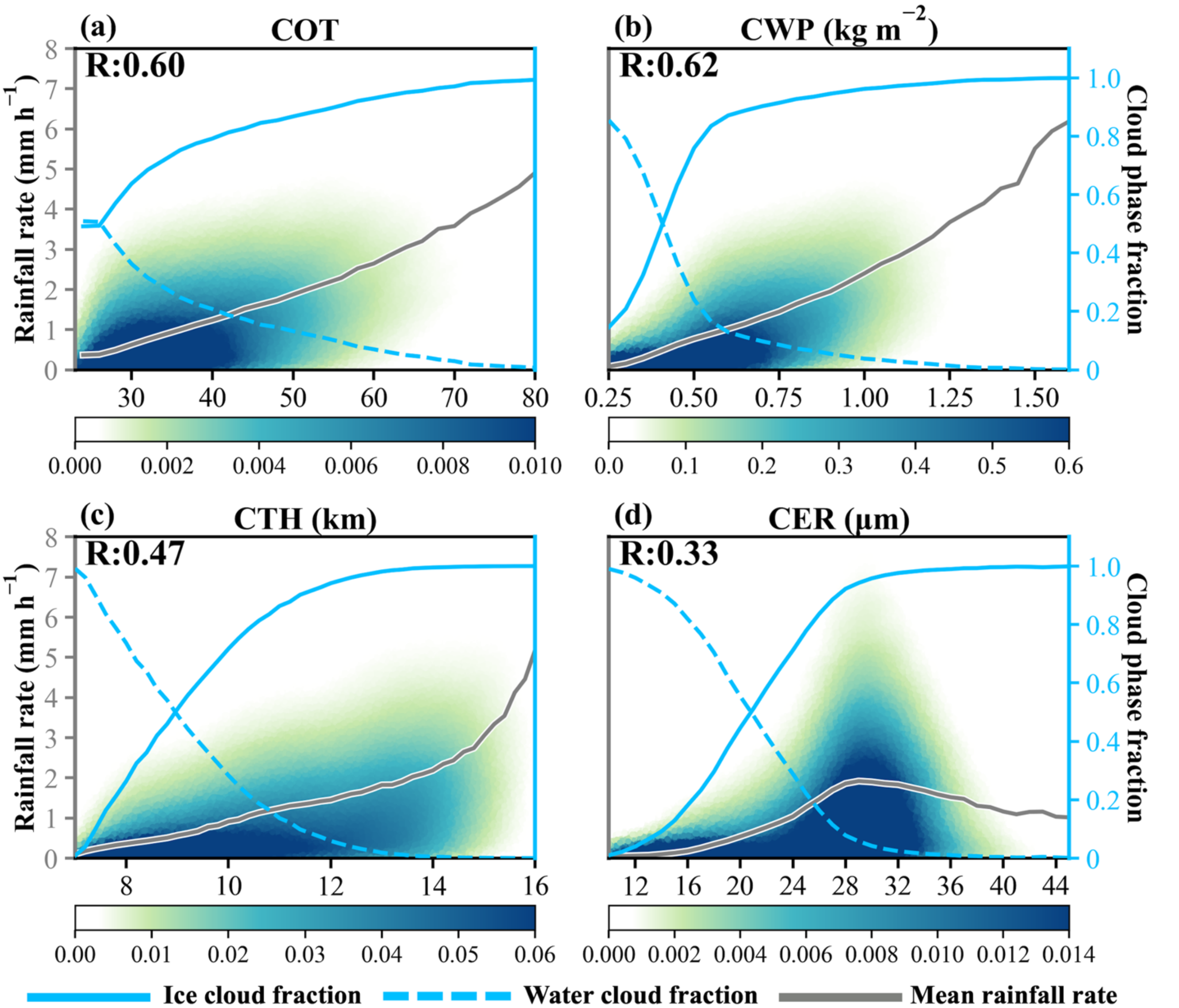

Figure 7. Scatter-density relationships between DCC cloud physical properties and RR across the whole study region. The panels show relationships between RR and COT (a), CWP (b), CTH (c), and CER (d).

240 The preceding results indicate that DCC rainfall is associated with large-scale meteorological backgrounds (Sect. 3.1) and cloud physical properties (Sects. 3.2 and 3.3). Based on these relationships, an RR estimation model was established to evaluate the potential of cloud physical properties for quantitative estimation of DCC RR. The model was based on eXtreme Gradient Boosting (XGBoost), which has strong capability in capturing nonlinear relationships (Chen and Guestrin, 2016), and was trained separately for the four subregions. Data from 2016–2018 were used for model training, data from 2019 were used as

245 an independent test set. The dataset division and hyperparameter settings are provided in Table A1.

https://doi.org/10.5194/egusphere-2026-4748
Preprint. Discussion started: 27 August 2026

Seven variables from three categories were finally used. The first category includes cloud physical property variables, containing CWP, CTH, and cloud horizontal area (AREA). CWP represents the total column hydrometeor content and serves as a material source for rainfall formation. CTH characterizes the vertical development of DCC, while AREA represents horizontal extent and reflects the influence of convective organization on RR (Li et al., 2021; Shusse and Tsuboki, 2006; Z. Zhao et al., 2025). The second category includes meteorological variables, containing TCWV and T2m. TCWV characterizes the column-integrated moisture supply, as deep convective rainfall generally requires sufficient moisture exceeding a certain threshold (Holloway and Neelin, 2009). T2m reflects near surface thermal conditions and the moisture-holding capacity of the lower atmosphere. The third category includes geographic location variables, containing the centroid latitude and longitude of DCC (LAT and LON). Given the pronounced spatial heterogeneity in rainfall mechanisms (Sects. 3.1 and 3.2), LAT and LON were included to allow the model to implicitly capture the effects of underlying surface type and local terrain.

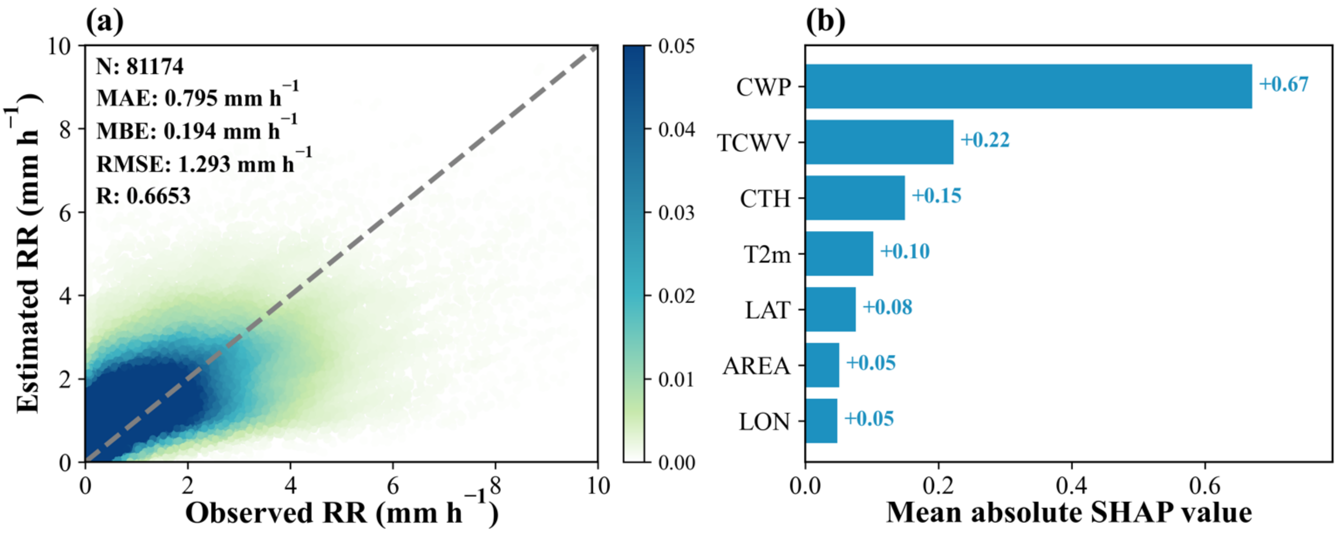

Figure 8. Scatter-density plot between estimated and observed RR across the whole study region (a). Feature importance of the input variables (b).

The evaluation results on the independent 2019 test set are presented in Fig. 8a and Table 2. The XGBoost-based model achieves reasonable RR estimation performance across the whole study region, with values of R, Mean Absolute Error (MAE), Mean Bias Error (MBE), and Root Mean Square Error (RMSE) of 0.6653, 0.795, 0.194, and 1.293, respectively. For the four subregions, models also maintain consistent performance, with R ranging from 0.6497 to 0.6603. The best performance is obtained over Region 1 (R = 0.6603), while the differences among the four subregions are relatively small. These results indicate that the selected feature set can capture the main variations in DCC RR. Feature importance analysis based on SHapley Additive exPlanations (SHAP; Fig. 8b; Table 2) shows that CWP is the dominant predictor across all subregions. This further supports the central role of CWP as the hydrometeor source for DCC rainfall. CTH and TCWV consistently rank among the top three predictors across all subregions, indicating that the vertical development of DCC and environmental moisture supply also provide important information for estimating DCC RR.

https://doi.org/10.5194/egusphere-2026-4748
Preprint. Discussion started: 27 August 2026

Table 2. Performance evaluation and feature importance of the XGBoost-based RR estimation models across the four subregions. Top 1–Top 3 denote three highest-ranking input variables.

Subregion	N	MAE ($mm\ h^{-1}$)	MBE ($mm\ h^{-1}$)	RMSE ($mm\ h^{-1}$)	R	Top 1	Top 2	Top 3
Region 1	24419	0.881	0.079	1.583	0.6603	CWP	TCWV	CTH
Region 2	20188	0.752	0.192	1.134	0.6497	CWP	TCWV	CTH
Region 3	13741	0.613	0.263	0.961	0.6596	CWP	CTH	TCWV
Region 4	22826	0.861	0.288	1.273	0.6545	CWP	TCWV	CTH

In addition to evaluating the quantitative RR estimation performance, we further examined whether the model could reconstruct the diurnal variations of DCC RR across the four subregions. This evaluation was performed using independent 2019 test set. Figure 9 shows clear regional differences in the reconstruction of RR diurnal variations. The model performs better in Regions 1 and 2, with R values of 0.89 and 0.95, respectively. It successfully captures the nighttime-to-morning increase in RR over the ocean and the pronounced afternoon peak over the eastern coastal region. In Region 3, the model captures the timing of the afternoon increase but generally overestimates its magnitude. In Region 4, the model fails to capture the early-morning peak associated with dynamical processes and terrain effects, which is reflected in the relatively low R value of 0.45. Moreover, the estimated RR is generally higher than the observed RR, consistent with the positive MBE shown in Table 2. In contrast, the maximum RR over the ocean is slightly underestimated. This bias pattern may be partly related to the skewed distribution of RR and the model's tendency to estimate the mean state, resulting in overestimation of weak rainfall and underestimation of strong rainfall. Overall, the model captures general RR diurnal features, including the thermally driven afternoon enhancement over land and the nighttime-to-morning enhancement over the ocean. However, its ability to reconstruct detailed diurnal features remains limited in terrain-influenced regions, where dynamic processes may play a more important role.

https://doi.org/10.5194/egusphere-2026-4748
Preprint. Discussion started: 27 August 2026

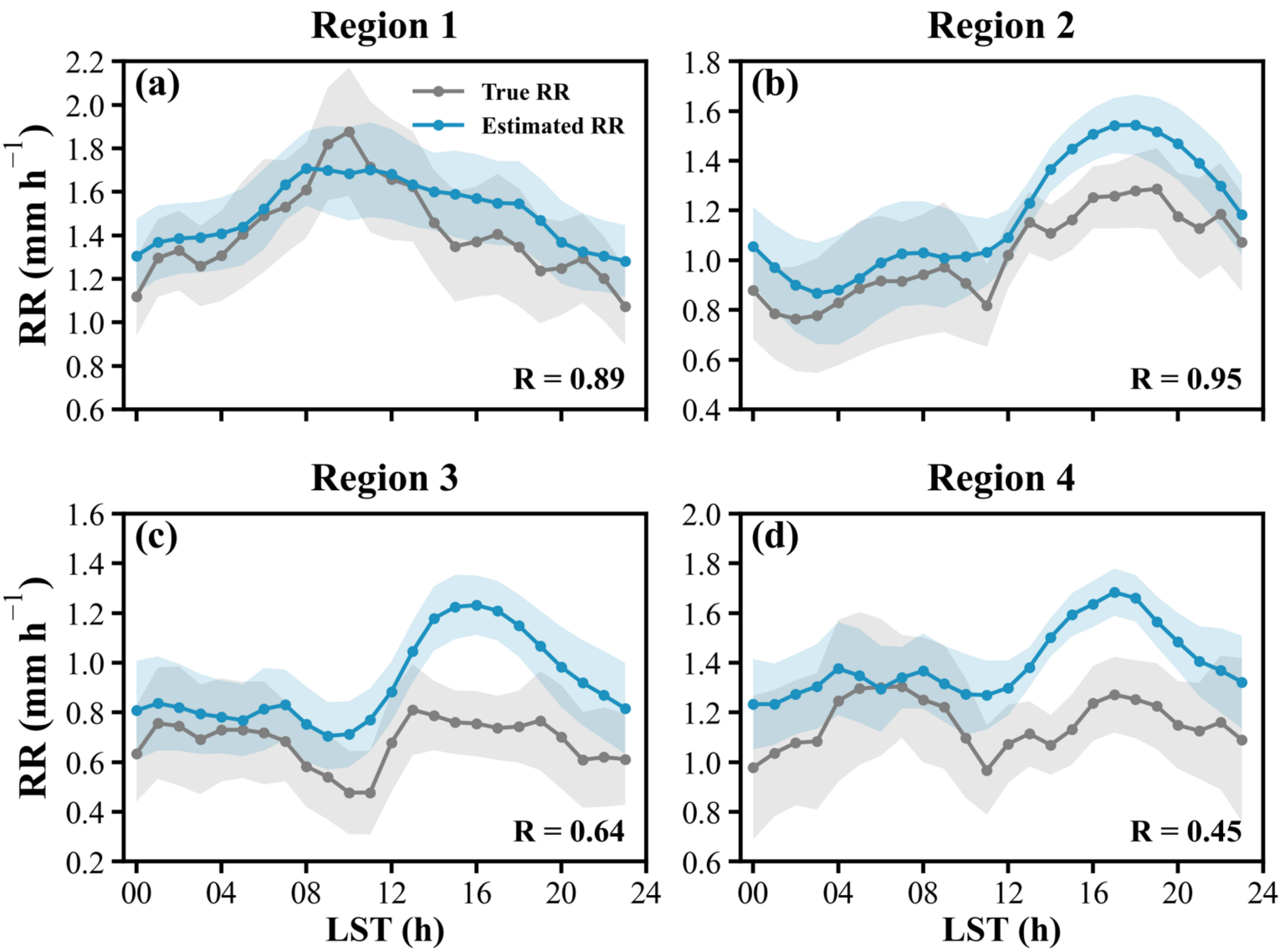

Figure 9. Reconstruction of diurnal variations in DCC RR across the four subregions.

4 Conclusion

Using all-day DaYu-CLAS cloud products and the TOOCAN-CPP method, this study automatically identified and tracked DCC over South China and the adjacent seas. To analyze the diurnal variations of DCC physical properties and their relationships with rainfall under different environmental backgrounds, the study region was divided into four subregions. The results show that DCC over the inland region (Region 3) exhibit a typical afternoon peak, which is likely associated with solar heating. Their activity begins to increase rapidly at around 10:00 LST and reaches its maximum during 15:00–18:00 LST. DCC over the eastern coastal area (Region 2) also show a single afternoon peak, but with a larger diurnal amplitude than that over the inland region. This stronger peak is likely associated with the combined effects of afternoon solar heating and sea breeze convergence. DCC over the southern flank of the Yungui Plateau (Region 4) exhibit distinctive bimodal patterns in RR, COT, and CWP. In addition to the afternoon thermodynamic peak associated with solar heating, the early morning dynamic

https://doi.org/10.5194/egusphere-2026-4748
Preprint. Discussion started: 27 August 2026

peak occurs at around 07:00 LST. This early morning peak is likely related to the joint effects of enhanced nocturnal LLJ activity and terrain effects. DCC over the oceanic region (Region 1) are active from nighttime to early morning, which may be associated with nocturnal cloud top longwave radiative cooling. Although the diurnal variations in DCC show pronounced regional heterogeneity, the relationships between cloud physical properties and RR show similar patterns across subregions. COT and CWP are strongly positively correlated with RR. CTH shows a nonlinear positive relationship with RR. CER exhibits a threshold-like behavior in its relationship with RR, with a transition occurring around 29 μm.

Based on these relationships, a XGBoost-based RR estimation model was further established by integrating cloud properties (CWP, CTH, and AREA), meteorological variables (TCWV and T2m), and geographic location information (LAT and LON). The model shows reasonable RR estimation performance across the four subregions ($R > 0.64$). Feature importance analysis further identifies CWP as the dominant predictor of RR estimation, while TCWV and CTH also provide important information. Moreover, the model reconstructs the general diurnal features of RR across different subregions, while some local variations, particularly those associated with specific dynamic processes, are not fully reproduced.

Overall, these findings improve the understanding of the diurnal variations of DCC over South China and the adjacent seas and demonstrate the application potential of cloud physical properties for strong convection monitoring and rainfall estimation. However, this study focused on South China and the adjacent seas, and future work will extend this analysis to broader regions by using all-day cloud products from global geostationary satellite observations, such as the Fengyun series, the Meteosat Second Generation (MSG) satellites, the Himawari series, and the Geostationary Operational Environmental Satellite (GOES) series, to further investigate the diurnal variations of DCC physical properties and their relationships with rainfall across different regions at the global scale.

https://doi.org/10.5194/egusphere-2026-4748
Preprint. Discussion started: 27 August 2026

Appendix A: Regional cloud-rainfall relationships and RR estimation model hyperparameter settings

Table A1. Dataset division and hyperparameter settings of XGBoost-based RR estimation model

Subregions	Dataset division		Hyperparameter settings		
	Training set (2016-2018)	Testing set (2019)	Max trees	Learning rate	Loss function
Region 1	69687	24419	1500	0.02	MSELoss
Region 2	59617	20188	1500	0.02	MSELoss
Region 3	38621	13741	1500	0.02	MSELoss
Region 4	68492	22826	1500	0.02	MSELoss
All regions	236417	81174	1500	0.02	MSELoss

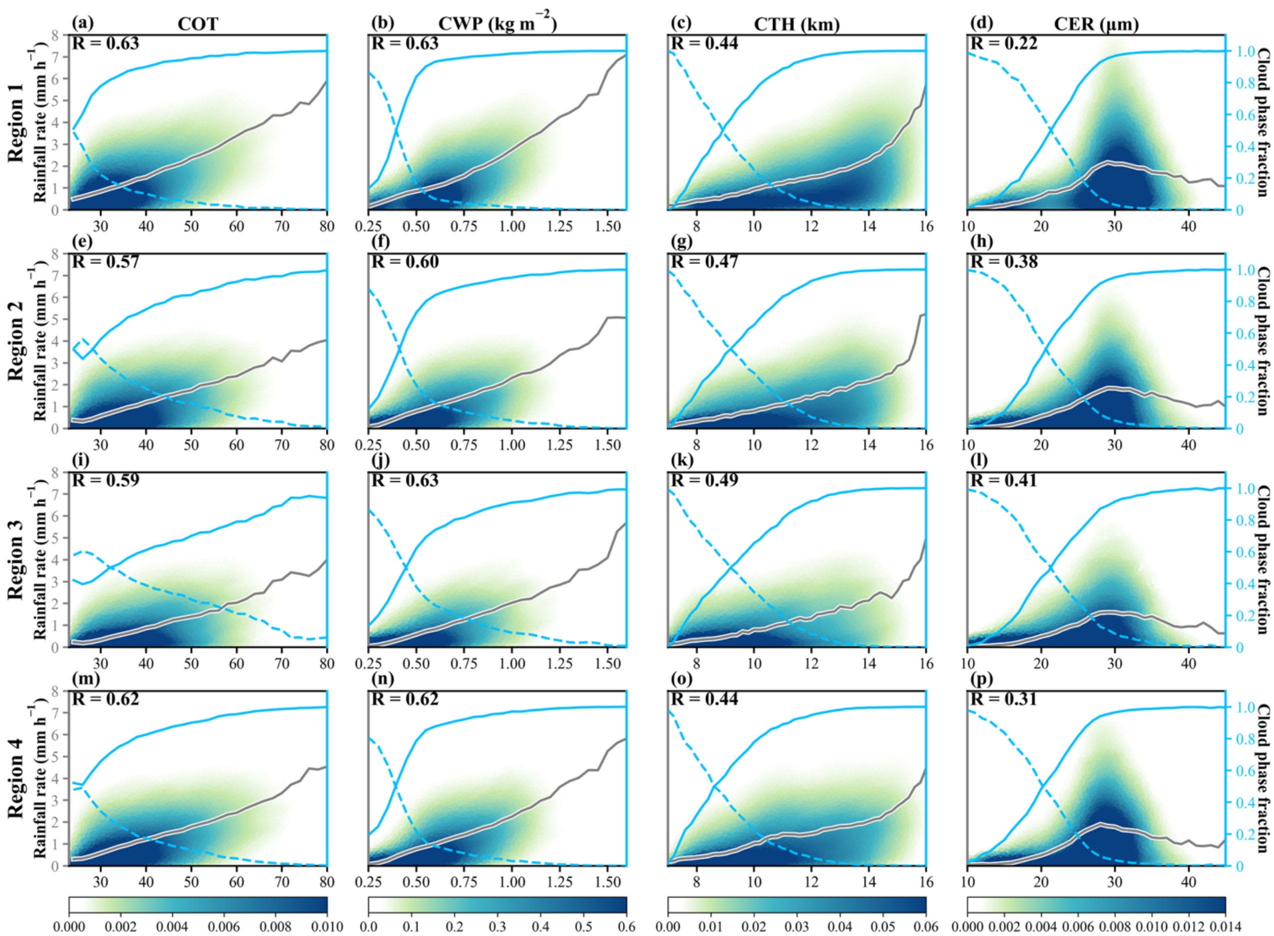

Figure A1. Scatter-density relationships between DCC cloud physical properties and RR across the four subregions. The panels show relationships between RR and COT (a, e, i, m), CWP (b, f, j, n), CTH (c, g, k, o), and CER (d, h, l, p).

https://doi.org/10.5194/egusphere-2026-4748
Preprint. Discussion started: 27 August 2026

Appendix B: Harmonic analysis

To quantitatively describe the diurnal variations in DCC characteristics, including frequency, rainfall amount, and rainfall rate, this study applies a cosine harmonic fitting method to the pixel-level diurnal time series. Previous studies have commonly represented the diurnal variations in rainfall, wind fields, or divergence using diurnal amplitude, daily mean, and phase terms, which characterize the diurnal intensity, mean state, and peak timing of the variable, respectively (Dai and Deser, 1999; Roy and Balling, 2005; Love et al., 2011).

In this study, DCC characteristics are calculated at a temporal interval of 30 min; therefore, one day is divided into 48 time steps. For each pixel (i,j) and each UTC time step, DCC frequency, DCC rainfall amount, and DCC rainfall rate are calculated separately. If a pixel is identified as DCC at a given time step, the DCC frequency for that pixel is increased by one. Meanwhile, the corresponding GPM rainfall rate at the DCC-affected pixel is extracted and used to calculate the DCC rainfall rate and DCC rainfall amount. For rainfall amount, the rainfall rate is multiplied by 0.5 h to represent the accumulated rainfall within the 30 min interval.

Because DCC diurnal variations are closely related to solar radiative forcing, UTC is converted to local solar time (LST) before the harmonic analysis:

$$t_{LST} = t_{UTC} + \frac{\lambda}{15}, \qquad \text{(B1)}$$

where λ is the longitude of the pixel in degrees, and both t_{UTC} and t_{LST} are expressed in hours. When $t_{\mathrm{LST}} > 24$ h, 24 h is subtracted so that the time is reset to the range of 0–24 h.

Subsequently, the diurnal time series $X(i,j,t)$ of each pixel is fitted using the first harmonic:

$$X(i,j,t) = A(i,j)\cos[\frac{2\pi}{24}(t - \phi(i,j)] + C(i,j)\ , \qquad \text{(B2)}$$

where $A(i,j)$ is the diurnal amplitude, representing the intensity of the diurnal variation; $\phi(i,j)$ is the phase, representing the peak time of the variable in the diurnal cycle; and $C(i,j)$ is the daily mean. The fitting procedure is applied separately to DCC frequency, DCC rainfall amount, and DCC rainfall rate, yielding the corresponding diurnal amplitude, peak time, and daily mean. Previous studies have also selected dominant harmonic components according to their research objectives. Since this study focuses primarily on the 24 h diurnal component of DCC characteristics, only the first harmonic is retained.

Data availability

The ERA5 reanalysis dataset is accessible through the Copernicus Climate Data Store (CDS): https://cds.climate.copernicus.eu/datasets. The GPM IMERG rainfall dataset can be accessed through NASA GES DISC: https://gpm1.gesdisc.eosdis.nasa.gov/data/GPM_L3/GPM_3IMERGHH.07/. The cloud physical property products are available from the Harvard Dataverse (Li, 2023): https://doi.org/10.7910/DVN/0FYANE. These products were developed

https://doi.org/10.5194/egusphere-2026-4748
Preprint. Discussion started: 27 August 2026

following the approaches described in Li et al. (2023) and Tong et al. (2023) and are incorporated into the DaYu Cloud Analysis System (DaYu-CLAS), which is accessible at https://fdu-crias.fudan.edu.cn/.

Author contributions

Feng Zhang: conceptualization, supervision, funding acquisition, methodology, writing – review and editing, writing – original draft; Zhiguo Wang: methodology, formal analysis, visualization, writing – original draft, writing – review and editing; Zhijun Zhao: data curation, validation, writing – review and editing, writing – original draft; Wenwen Li: validation, data curation, writing – review and editing; Zhixin Yang: data curation, visualization, writing – review and editing;

Competing interests

The authors declare that they have no conflict of interest.

Acknowledgements

The authors thank the Copernicus Climate Data Store for providing the ERA5 reanalysis data and NASA GES DISC for providing the GPM IMERG rainfall data used in this study. The authors also acknowledge the DaYu-CLAS team for providing cloud physical property products and acknowledge the CFFF platform of Fudan University for providing computational resources used in this research.

Financial support

This work is supported in part by the National Key Research and Development Program of China (Grant 2024YFF0808303); in part by Shanghai Pilot Program for Basic Research–Fudan University (Grant 21TQ1400100 (25TQ008)); and in part by the Zhejiang Provincial Natural Science Foundation of China (Grant LQN25D050004).

References

Andreae, M. O., Afchine, A., Albrecht, R., Holanda, B. A., Artaxo, P., Barbosa, H. M. J., Borrmann, S., Cecchini, M. A., Costa, A., Dollner, M., Fütterer, D., Järvinen, E., Jurkat, T., Klimach, T., Konemann, T., Knote, C., Krämer, M., Krisna, T., Machado, L. A. T., Mertes, S., Minikin, A., Pöhlker, C., Pöhlker, M. L., Pöschl, U., Rosenfeld, D., Sauer, D., Schlager, H., Schnaiter, M., Schneider, J., Schulz, C., Spanu, A., Sperling, V. B., Voigt, C., Walser, A., Wang, J., Weinzierl, B., Wendisch, M., and Ziereis, H.: Aerosol characteristics and particle production in the upper troposphere over the Amazon Basin, Atmos. Chem. Phys., 18, 921–961, https://doi.org/10.5194/acp-18-921-2018, 2018.

Barth, M. C., Kim, S.-W., Wang, C., Pickering, K. E., Ott, L. E., Stenchikov, G., Leriche, M., Cautenet, S., Pinty, J.-P., Barthe, Ch., Mari, C., Helsdon, J. H., Farley, R. D., Fridlind, A. M., Ackerman, A. S., Spiridonov, V., and Telenta, B.: Cloud-scale model intercomparison of chemical constituent transport in deep convection, Atmos. Chem. Phys., 7, 4709–4731, https://doi.org/10.5194/acp-7-4709-2007, 2007.

Cattani, E., Torricella, F., Laviola, S., and Levizzani, V.: On the statistical relationship between cloud optical and microphysical characteristics and rainfall intensity for convective storms over the Mediterranean, Nat. Hazards Earth Syst. Sci., 9, 2135–2142, https://doi.org/10.5194/nhess-9-2135-2009, 2009.

Chen, G., Sha, W., and Iwasaki, T.: Diurnal variation of precipitation over southeastern China: Spatial distribution and its seasonality, J. Geophys. Res.-Atmos., 114, 2008JD011103, https://doi.org/10.1029/2008JD011103, 2009.

Chen, T. and Guestrin, C.: XGBoost: A Scalable Tree Boosting System, in: Proceedings of the 22nd ACM SIGKDD International Conference on Knowledge Discovery and Data Mining, KDD '16: The 22nd ACM SIGKDD International Conference on Knowledge Discovery and Data Mining, 785–794, https://doi.org/10.1145/2939672.2939785, 2016.

Chen, X., Zhang, F., and Zhao, K.: Diurnal Variations of the Land–Sea Breeze and Its Related Precipitation over South China, J. Atmos. Sci., 73, 4793–4815, https://doi.org/10.1175/JAS-D-16-0106.1, 2016.

Dai, A. and Deser, C.: Diurnal and semidiurnal variations in global surface wind and divergence fields, J. Geophys. Res.-Atmos., 104, 31109–31125, https://doi.org/10.1029/1999JD900927, 1999.

Feng, Z., Dong, X., Xi, B., McFarlane, S. A., Kennedy, A., Lin, B., and Minnis, P.: Life cycle of midlatitude deep convective systems in a Lagrangian framework, J. Geophys. Res.-Atmos., 117, 2012JD018362, https://doi.org/10.1029/2012JD018362, 2012.

Feng, Z., Leung, L. R., Liu, N., Wang, J., Houze, R. A., Li, J., Hardin, J. C., Chen, D., and Guo, J.: A Global High-Resolution Mesoscale Convective System Database Using Satellite-Derived Cloud Tops, Surface Precipitation, and Tracking, J. Geophys. Res.-Atmos., 126, e2020JD034202, https://doi.org/10.1029/2020JD034202, 2021.

Fiolleau, T. and Roca, R.: An Algorithm for the Detection and Tracking of Tropical Mesoscale Convective Systems Using Infrared Images From Geostationary Satellite, IEEE Trans. Geosci. Remote Sens., 51, 4302–4315, https://doi.org/10.1109/TGRS.2012.2227762, 2013.

Guo, Z. and Zhou, T.: Seasonal variation and physical properties of the cloud system over southeastern China derived from CloudSat products, Adv. Atmos. Sci., 32, 659–670, https://doi.org/10.1007/s00376-014-4070-y, 2015.

Holloway, C. E. and Neelin, J. D.: Moisture Vertical Structure, Column Water Vapor, and Tropical Deep Convection, J. Atmos. Sci., 66, 1665–1683, https://doi.org/10.1175/2008JAS2806.1, 2009.

Houze, R. A.: Observed structure of mesoscale convective systems and implications for large-scale heating, Q. J. Roy. Meteor. Soc., 115, 425–461, https://doi.org/10.1002/qj.49711548702, 1989.

Houze, R. A.: Mesoscale convective systems, Rev. Geophys., 42, 2004RG000150, https://doi.org/10.1029/2004RG000150, 2004.

https://doi.org/10.5194/egusphere-2026-4748
Preprint. Discussion started: 27 August 2026

Kawamoto, K., Nakajima, T., and Nakajima, T. Y.: A Global Determination of Cloud Microphysics with AVHRR Remote Sensing, J. Climate, 14, 2054–2068, https://doi.org/10.1175/1520-0442(2001)014%3C2054:AGDOCM%3E2.0.CO;2, 2001.

Kikuchi, M. and Suzuki, K.: Characterizing Vertical Particle Structure of Precipitating Cloud System From Multiplatform Measurements of A-Train Constellation, Geophys. Res. Lett., 46, 1040–1048, https://doi.org/10.1029/2018GL081244, 2019.

Kong, H., Zhang, Q., Du, Y., and Zhang, F.: Characteristics of Coastal Low-Level Jets Over Beibu Gulf, China, During the Early Warm Season, J. Geophys. Res.-Atmos., 125, e2019JD031918, https://doi.org/10.1029/2019JD031918, 2020.

Kubar, T. L. and Hartmann, D. L.: Vertical structure of tropical oceanic convective clouds and its relation to precipitation, Geophys. Res. Lett., 35, 2007GL032811, https://doi.org/10.1029/2007GL032811, 2008.

Lee, J.-D., Wu, C.-C., and Ito, K.: Diurnal Variation of the Convective Area and Eye Size Associated with the Rapid Intensification of Tropical Cyclones, Mon. Weather Rev., 148, 4061–4082, https://doi.org/10.1175/MWR-D-19-0345.1, 2020.

Li, J.: Himawari-8 Cloud Properties Datasets (1.0), https://doi.org/10.7910/DVN/0FYANE, 2023.

Li, J., Zhang, F., Li, W., Tong, X., Pan, B., Li, J., Lin, H., Letu, H., and Mustafa, F.: Transfer-Learning-Based Approach to Retrieve the Cloud Properties Using Diverse Remote Sensing Datasets, IEEE Trans. Geosci. Remote Sens., 61, 1–10, https://doi.org/10.1109/TGRS.2023.3318374, 2023.

Li, W., Zhang, F., Yu, Y., Iwabuchi, H., Shen, Z., Wang, G., and Zhang, Y.: The semi-diurnal cycle of deep convective systems over Eastern China and its surrounding seas in summer based on an automatic tracking algorithm, Clim. Dyn., 56, 357–379, https://doi.org/10.1007/s00382-020-05474-1, 2021.

Lin, B., Xu, K., Minnis, P., Wielicki, B. A., Hu, Y., Chambers, L., Fan, T., and Sun, W.: Coincident occurrences of tropical individual cirrus clouds and deep convective systems derived from TRMM observations, Geophys. Res. Lett., 34, 2007GL029768, https://doi.org/10.1029/2007GL029768, 2007.

Liou, K.-N.: An introduction to atmospheric radiation, 2nd ed., Academic Press, Amsterdam ; Boston, 583 pp., 2002.

Liu, C., Zhang, F., Ouyang, H., Li, W., and Zhao, Z.: Diurnal Variation of Cloud Physical Properties for Tropical Cyclones Over North Atlantic in 2019–2023, Geophys. Res. Lett., 52, e2025GL115566, https://doi.org/10.1029/2025GL115566, 2025.

Love, B. S., Matthews, A. J., and Lister, G. M. S.: The diurnal cycle of precipitation over the Maritime Continent in a high-resolution atmospheric model, Q. J. Roy. Meteor. Soc., 137, 934–947, https://doi.org/10.1002/qj.809, 2011.

Masunaga, H.: A Satellite Study of Tropical Moist Convection and Environmental Variability: A Moisture and Thermal Budget Analysis, J. Atmos. Sci., 70, 2443–2466, https://doi.org/10.1175/JAS-D-12-0273.1, 2013.

Nakajima, T. Y. and Nakajma, T.: Wide-Area Determination of Cloud Microphysical Properties from NOAA AVHRR Measurements for FIRE and ASTEX Regions, J. Atmos. Sci., 52, 4043–4059, https://doi.org/10.1175/1520-0469(1995)052%3C4043:WADOCM%3E2.0.CO;2, 1995.

Phadtare, J. and Bhat, G. S.: Characteristics of Deep Cloud Systems under Weak and Strong Synoptic Forcing during the Indian Summer Monsoon Season, Mon. Weather Rev., 147, 3741–3758, https://doi.org/10.1175/MWR-D-18-0346.1, 2019.

Rickenbach, T. M. and Rutledge, S. A.: Convection in TOGA COARE: Horizontal Scale, Morphology, and Rainfall Production, J. Atmos. Sci., 55, 2715–2729, https://doi.org/10.1175/1520-0469(1998)055%3C2715:CITCHS%3E2.0.CO;2, 1998.

Roca, R., Bergès, J.-C., Brogniez, H., Capderou, M., Chambon, P., Chomette, O., Cloché, S., Fiolleau, T., Jobard, I., Lémond, J., Ly, M., Picon, L., Raberanto, P., Szantai, A., and Viollier, M.: On the water and energy cycles in the Tropics, C. R. Geosci., 342, 390–402, https://doi.org/10.1016/j.crte.2010.01.003, 2010.

Roy, S. S. and Balling, R. C.: Analysis of Diurnal Patterns in Winter Precipitation across the Conterminous United States, Mon. Weather Rev., 133, 707–711, https://doi.org/10.1175/MWR-2873.1, 2005.

Shusse, Y. and Tsuboki, K.: Dimension Characteristics and Precipitation Efficiency of Cumulonimbus Clouds in the Region Far South from the Mei-Yu Front over the Eastern Asian Continent, Mon. Weather Rev., 134, 1942–1953, https://doi.org/10.1175/MWR3159.1, 2006.

Simpson, M., Warrior, H., Raman, S., Aswathanarayana, P. A., Mohanty, U. C., and Suresh, R.: Sea-breeze-initiated rainfall over the east coast of India during the Indian southwest monsoon, Nat. Hazards, 42, 401–413, https://doi.org/10.1007/s11069-006-9081-2, 2007.

Steiner, M., Houze, R. A., and Yuter, S. E.: Climatological Characterization of Three-Dimensional Storm Structure from Operational Radar and Rain Gauge Data, J. Appl. Meteorol., 34, 1978–2007, https://doi.org/10.1175/1520-0450(1995)034%3C1978:CCOTDS%3E2.0.CO;2, 1995.

Su, L., Bai, L., Zhang, S., Chen, G., and Du, Y.: Day-Night and Land-Sea Contrasts of Upscale Convective Growths at Coastal South China, J. Geophys. Res.-Atmos., 130, e2024JD042643, https://doi.org/10.1029/2024JD042643, 2025.

Tong, X., Li, J., Zhang, F., Li, W., Pan, B., Li, J., and Letu, H.: The Deep-Learning-Based Fast Efficient Nighttime Retrieval of Thermodynamic Phase From Himawari-8 AHI Measurements, Geophys. Res. Lett., 50, e2022GL100901, https://doi.org/10.1029/2022GL100901, 2023.

Xiao, H., Zhang, F., Wang, L., Pan, B., Zhu, Y., Wang, M., Li, W., Guo, B., and Li, J.: High-resolution ensemble retrieval of cloud properties for all-day based on geostationary satellite, npj Clim. Atmos. Sci., 8, 386, https://doi.org/10.1038/s41612-025-01263-x, 2025.

Xu, W.: Precipitation and Convective Characteristics of Summer Deep Convection over East Asia Observed by TRMM, Mon. Weather Rev., 141, 1577–1592, https://doi.org/10.1175/MWR-D-12-00177.1, 2013.

Zhao, L., Zhang, F., Zhao, Z., Lu, F., Li, J., Guo, B., and Li, W.: All-day global cloud physical properties products with 0.07° resolution retrieved from geostationary satellite imagers covering the period from 2000 to 2022, Earth Syst. Sci. Data, 18, 1813–1832, https://doi.org/10.5194/essd-18-1813-2026, 2026.

Zhao, Y., Li, J., Wen, D., Li, Y., Wang, Y., and Huang, J.: Distinct structure, radiative effects, and precipitation characteristics of deep convection systems in the Tibetan Plateau compared to the tropical Indian Ocean, Atmos. Chem. Phys., 24, 9435–9457, https://doi.org/10.5194/acp-24-9435-2024, 2024.

Zhao, Z., Zhang, F., Wu, Q., Li, Z., Tong, X., Li, J., and Han, W.: Cloud Identification and Properties Retrieval of the Fengyun-4A Satellite Using a ResUnet Model, IEEE Trans. Geosci. Remote Sens., 61, 1–18, https://doi.org/10.1109/TGRS.2023.3252023, 2023.

https://doi.org/10.5194/egusphere-2026-4748
Preprint. Discussion started: 27 August 2026

Zhao, Z., Zhang, F., Li, W., and Li, J.: Image-Based Retrieval of All-Day Cloud Physical Parameters for FY4A/AGRI and Its Application Over the Tibetan Plateau, J. Geophys. Res.-Atmos., 129, e2024JD041032, https://doi.org/10.1029/2024JD041032, 2024.

Zhao, Z., Zhang, F., Li, W., Yang, B., He, Q., Fu, H., and Cai, M.: Identification and Tracking of Deep Convection Systems Over the Tibetan Plateau and Its Surrounding Areas in Summer Using All-Day Cloud Physical Properties, Geophys. Res. Lett., 52, e2025GL118433, https://doi.org/10.1029/2025GL118433, 2025.

Zheng, X., Yang, Y., Yuan, Y., Cao, Y., and Gao, J.: Comparison of Macro- and Microphysical Properties in Precipitating and Non-Precipitating Clouds over Central-Eastern China during Warm Season, Remote Sens., 14, 152, https://doi.org/10.3390/rs14010152, 2021.

Zheng, Y.-G. and Chen, J.: A climatology of deep convection over South China and the adjacent waters during summer, J. Trop. Meteorol., 19, 1–15, https://doi.org/10.16555/j.1006-8775.2013.01.002, 2013.